# The MRItab: A MR-compatible touchscreen with video-display

Sophia Vinci-Booher, Jeffrey Sturgeon, Thomas James, Karin James*

*Department of Psychological and Brain Sciences at Indiana University, United States*

## ABSTRACT

*Background:* A touchscreen interface permits rich user interactions for research in many fields, but is rarely found within a Magnetic Resonance Imaging (MRI) environment due to difficulties adapting conventional technologies to the strong electromagnetic fields. Conventional MR-compatible video display technology uses either large-screen displays that are placed outside of the bore of the MRI itself, or projectors located beyond the participant's reach, making touch interfaces impossible.

*New method:* Here, we describe the MR-compatibility of the 'MRItab' in terms of MR safety and image quality. The MRItab adapts inexpensive off-the-shelf components with special signal-driver circuitry and shielding to bring the touchscreen interface into the MR environment, without adversely affecting MRI image quality, thereby making touch interfaces possible.

*Results:* Our testing demonstrated that the functioning of the MRItab was not affected by the functioning of the MRI scanner and that the MRItab did not adversely affect the image data acquired. Participants were able to interact naturally with the MRItab during MRI scanning.

*Comparison with other method (s):* The MRItab is the first MR-compatible touchscreen device with video-display screen capabilities designed for use in the MRI environment. This interactive digital device is the first to allow participants to see their hands directly as they interact with a touch-sensitive display screen, resulting in high ecological validity.

*Conclusions:* The MRItab provides a methodological advantage for research in many fields, given the realistic human-computer interaction it supports.

## 1. Introduction

Touchscreen tablet technologies have become a major component of daily life. People are constantly interacting with tablets, including phones, in ways that require real-time user–tablet interactions. Tablets have also become a crucial component of research itself, becoming an invaluable tool for stimulus presentation and response collection. The use of computer tablets in research settings permits the use of a large variety of stimuli, such as video and interactive modules, and enables recording and playback of a participant's actions. Erasing is faster and more flexible and background images may be more easily changed than with physical media. The computer tablet, in short, has changed the way humans gain knowledge and communicate. It has also changed research by combining the processing power of a computer with a user-controlled screen. Until now, there has been no way of knowing the effects that this human-computer interaction has on underlying human neurocognitive function.

The mechanisms that underlie human behavior can be measured using Functional Magnetic Resonance Imaging (fMRI), which allows the researcher to measure changes in brain function in response to a task as they occur in real time. One limitation of MR-based techniques, however, is that they use strong magnetic fields to acquire images. Apparatuses used to experimentally manipulate cognitive demands that are placed in the MRI bore with the subject during functional imaging must be "magnet compatible" – they must contain neither ferromagnetic materials (MR-safe) nor non-ferromagnetic components that reduce image quality (MR-compatible). For interactive MR-compatible devices, we feel there is an additional criterion that interaction must be easy for the subject. For use in cognitive neuroscience experiments with human participants, interactive devices must, therefore, be MR-safe, MR-compatible, and participant-friendly. For these reasons, the development of an interactive touchscreen device with video-display capabilities – a device that simulates the user-experience of a common commercial tablet (e.g., iPad, Android) – that is useable in the MR-environment has remained elusive, making the study of ecologically valid human-computer interactions with fMRI impossible thus far.

Despite these hurdles, the design of MR-compatible touchscreens has received considerable attention, and several versions have

* Corresponding author at: 1101 E. 10th St, Bloomington, IN 47405-7007, United States.
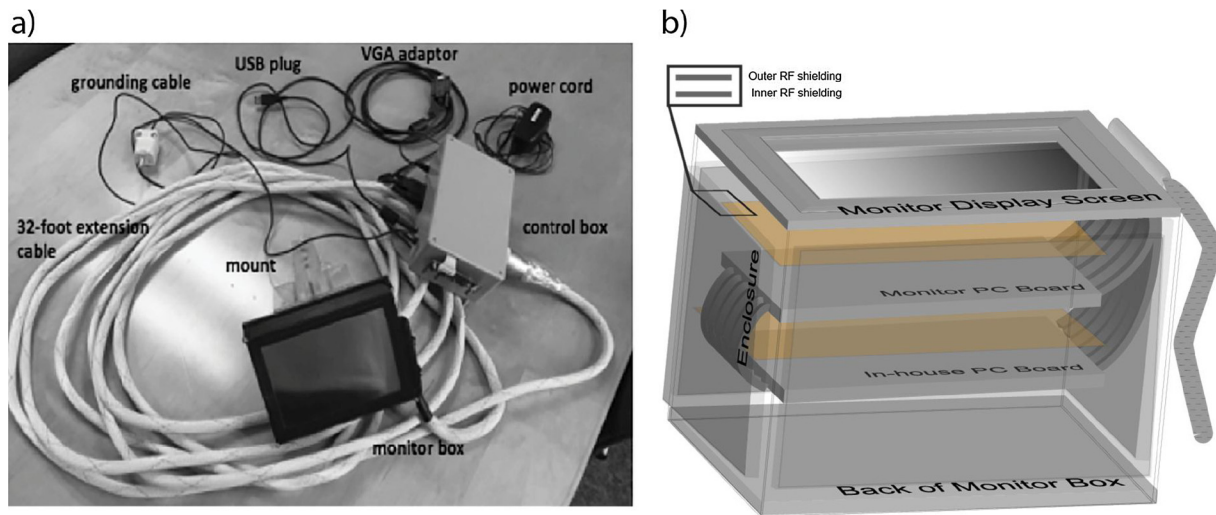 *E-mail address:* khjames@indiana.edu (K. James).

**Fig. 1.** (a) *Components of the MRItab*. The MRItab contains a MR-compatible video-display touchscreen connected to a non-MR-compatible control box by an MR-compatible extension cable. For use, the control box must be plugged into a computer via the VGA adaptor. (b) *Components within the Monitor Box*. The Monitor Box contained two PC driver boards walled in by an Enclosure. The Monitor PC Board was the standard board that came with the display screen (see Device Description for more information). We constructed the In-house PC Board. The Enclosure contained six double-walled fiberglass surfaces that were electrically joined at the edges to create two RF shielding layers, an inner RF shield and an outer RF shield. RF paper, indicated by orange color, was placed between each layer of components within the Enclosure for extra RF shielding.

appeared, although none have display capabilities. There were two general types of touchscreens that were explored. The ShapeTape ™ (Mraz et al., 2004) was the first of this kind of device and relied on fiber optic cables and sensors that track the position of a stylus that is in contact with the touchscreen. A version with higher spatial and temporal resolution was implemented in 2011 (Tam et al.). The second type of touchscreen made use of a light-emitting pen whose trajectory on a white paper surface could be captured by a camera on the other side of the writing surface placed several meters away (Diciotti et al., 2010). A similar version was implemented in 2013 that has a higher spatial and temporal resolution (Reitz et al., 2013). Although these devices allow participants to interact with a writing surface that records writing trajectories, they do not allow the user to receive visual feedback in real time on the device itself. All visual feedback must be presented on a separate surface, often projected onto a mirror above their heads. They allow measurement of the motor actions of a participant on the tablet-like surface, but cannot produce the visual feedback to the participant that is necessary for ecological validity. Real-time interaction is a crucial component of the human-tablet interaction that is necessary for a full understanding of the impact of these devices on neurocognitive function.

De-coupling of motor production from the resultant visual percept (as seen with the previous tablet-like apparatuses) presents difficulties for studies where the use of vision to guide action is important. In research studying the neural responses during gaming behaviors, for instance, the coupling between vision and action is crucial to ecologically valid tablet/phone interfacing, virtual spatial navigation, and any work that requires visually guided responses based on motor production. One area of research that requires visually guided action is the study of manual symbol production. Ecologically valid handwriting, for example, has been difficult to replicate in MR environments due to an inability to provide participants with real-time visual feedback about the location of their hand relative to the writing surface and the current trajectory of their writing. There have been a number of creative attempts to study the neural systems supporting handwriting. Participants have been asked to write letters with their finger in the air (Katanoda et al., 2001), on a paper tablet by their waist (James and Gauthier, 2006), or on a recording device that can project what participants write onto a mirror above their head with (Karimpoor et al., 2015), or without (Tam et al., 2011), a virtual hand avatar. Although innovative,

these methods are not able to capture handwriting as a visually guided action, because these methods do not allow participants to see their physical hand and the letter produced as they are writing it on the surface onto which they are writing it during fMRI neuroimaging.

MR-compatible touchscreens have allowed researchers and clinicians to record user-input, such as handwriting trajectories written on the touchscreen, but any visual feedback provided to the participant must still be provided via large-screen displays that are placed outside of the bore or via mirrored projections. No MR-compatible devices have paired video-display with a touchscreen interface. Current devices are, therefore, only able to record user input and remain unable to reproduce the rich user-tablet interactions that have become so integral to daily life. Here, we describe the development and validation of an MR-compatible electronic writing device with both touchscreen and video-display capabilities that mimic the user-experience of common commercial tablets: the MRItab.

## 2. Materials and methods

### 2.1. Device description: the MRItab

Our approach was to utilize existing technology and easily attainable materials as much as possible. We used an off-the-shelf display screen and touch overlay, because those components are generally the most difficult to manufacture in-house. Initial experiments involved disassembling normal computer monitors, removing ferrous components, and testing for MRI-safety and functionality. We first determined the MR-safety of all components of a conventional video-display screen. MR-safe components were left inside the tablet and all non-MR-safe components were moved to a control box that did not enter into the MR environment.

Our plan from the outset was to make an extension cable to put as much distance between the Monitor Box in the MRI environment and the ferrous components used to drive it in the Control Box. The Extension Cable was 9.75 m long and passed through the penetration panel that separated the room containing the MRI from the control room. Most control boards that were required to receive input from the touchscreen and project output to the display screen were grouped together inside the Control Box while a few necessary circuit boards were placed inside the Monitor Box.

**Fig. 2.** Use of the MRItab with holding apparatus.

The components of the MRItab are displayed in Figs. 1 and 2. Each component is described in turn. From our experience with the current version of the MRItab, we believe the life expectancy to be around 3 years if the device were used several times each week.

### 2.1.1. Monitor Box

*2.1.1.1. LCD monitor.* A 18-cm, 1280 × 800 IPS LCD monitor by Tontec was used for video-display. Its driver board allows for VGA, HDMI, and analog audio inputs. The MRItab, however, only used the VGA input. There were many similarly sized and priced monitors, but this particular unit was selected for the configuration used in its video driver cable. While some display screens utilized ribbon cables consisting of 40 or more conductors, the model we selected used a different low voltage digital signal (LVDS) scheme that accomplished the same result using less than 20 conductors. Both circuit boards, the in-house custom PC board and the monitor driver board, were contained within the Monitor Box (Fig. 1).

*2.1.1.2. Touchscreen overlay.* The MRItab made use of a touchscreen surface similar to that of Tam et al. (2011) placed atop a novel MR-safe display screen. We chose to model our touchscreen surface after that of Tam et al. (2011) because of its superior spatial and temporal resolution. The touch overlay was a resistive four-wire type. The USB converter and driver software were from Adafruit.

*2.1.1.3. Enclosure.* The Enclosure provided RF shielding as well as structurally encasing the LCD monitor and PC boards in the Monitor Box. The Enclosure was constructed primarily of 17.5 μm thick copper clad on both sides FR-4 composite material, more commonly referred to as circuit board material. The sides were joined together on the interior and exterior using soldered copper tape and conductive epoxy. The front of the Enclosure had a rectangular hole milled out to expose the video-display screen.

As all magnetic shielding materials available to us were themselves ferrous materials, there was really no magnetic shielding. The materials in the Enclosure were, therefore, exposed to the magnetic field. The amount of material that would experience magnetic interference was very small and included less than 0.5 g in the form of 4 inductors isolated from each other, all deeply imbedded within the board. To reduce the likelihood that the components within the Monitor Box would experience magnetic interference, we positioned the Monitor Box within a specific range of locations within the bore to ensure that the components within the Monitor Box experienced the least amount of magnetic field change possible. The range of acceptable positions were found through trial and error and generally required that the MRItab be positioned perpendicular to the static magnetic field and within 0.5–1.0 m of isocenter. In regards to magnetic pull, the weight of the Monitor Box rendered the small magnetic pull generated by the small amount of ferrous materials inside the Monitor Box ineffective.

### 2.1.2. Control box

Many of the components within the Control Box were non-MR-safe components and, therefore, the Control Box could not enter into the MRI room.

The Control Box contained several driver boards for the video-display, including the mating

driver board to the LVDS/LCD display screen and a custom driver PC board with five DS25br120TSD/N0PB driver chips that both connected to the custom PC board in the Monitor Box. The driver board for the LVDS/LCD was a 150 mm to 200 mm display driver board that connected to the VGA AVI AT070TN90/92/94 LVDS board. The custom driver PC board supported voltage regulation and filtering for driving the LCD monitor back lighting. The voltage regulation also kept the driver chips stable and reduced any RF noise received from the MR environment. These driver chips stabilized and boosted the weak signals from the LCD driver board before sending them down balanced 100-Ohm twisted-pair wires to the LCD display receiving board.

The Control Box also contained an Adafruit AR1100 touchscreen driver board that supported touchscreen pass-through for recording touchscreen inputs. Note that the touchscreen itself was a generic resistive-type touchscreen. The touchscreen signals passed through the LCD driver board and then connected to the Adafruit AR1100 touchscreen driver board before connecting to an external computer via a USB mini connector and cable.

There were four ports mounted to the outside of the Control Box: the power supply, VGA, USB, and grounding ports. The LCD controls were also mounted to the outside of the box and allowed users to select parameters of the visual display, similar to options regularly available with standard projectors (e.g., brightness, contrast).

### 2.1.3. Extension cable

The 9.75-meter extension cable passed through the penetration panel that separates the room containing the MRI from the control room. The cable, commonly referred to as Category 7 (CAT 7), had several desirable properties; specifically, it contained multiple twisted pair construction with shields for each pair and an additional shield covered all pairs. CAT 7 cable is generally sold for use as Ethernet cable and, thus, contains 4 pairs of wires with a common shield and a RJ-45 connector on each end. To connect the shields of multiple cables to each other, the cables were hard-wired to the touchscreen instead of the standard RJ-45 connections inside the Monitor Box.

For the touch overlay, each wire was sent along the extension cable from the touchscreen side in the Monitor Box to the driver board side in the Control Box. No special driver circuitry was used for the touch overlay cable, just a passive extension.

LVDS, commonly used for high-speed signals such as those found in video, was used to send signals along the cable. Cable driver chips were placed at both ends of our custom cable to enforce proper impedance matching and timing characteristics to reduce interference over the

**Fig. 3.** The holding apparatus.
The 'cage' apparatus allows for subject-specific locations by holding the MRItab at an individualized location. Locations will differ for children (top right) and adults (bottom right), for example. The cage apparatus also allows for the removal of the MRItab during a scanning session, in cases where that is desirable.

9.75-meter cable run.[1] The cable driver chips were mounted on in-house custom PC board and connected via ribbon cable to the monitor hardware board in the Monitor Box. The driver-board end in the Control Box was terminated with a circular 24-pin connector.

### 2.1.4. Power supply

Power was only needed to control the signals going into the monitor and the display itself. One small 5 V DC power supply, housed inside the Control Box, provided power to the LVDS driver circuitry. Upon reaching the in-house custom PC board, the voltage was regulated down to 3 V. The power supply was transformer isolated from the building to ensure that there was no physical connection with the main power supply of the building. This ensured that the voltage would never be greater than expected.

### 2.1.5. Holding apparatus and set-up

Special attention was paid to the apparatus and set-up given the restricted space inside the bore of the MRI. The standard MRI bore is 60 cm in diameter and the adult 'bust depth' range is roughly 17.4–23.6 cm for women and 21.8–28.2 cm for men. The Monitor Box was positioned so that the long edge (17.78 cm) ran parallel to the horizontal surface of the scanner bed and so that the short edge (12.70 cm) ran perpendicular to that surface (Fig. 3).[2] This leaves just enough room for a participant's chest cavity.

The MRItab had a mounting system that could be slid into the track of the 'cage' to that the MRItab could be positioned at a location that maximized the comfort of the participant, the visibility of the display screen, and the ability of the participant to write on the MRItab (Fig. 3). The cage was held in place by Velcro strips on the scanner bed and on the base of the cage.

### 2.1.6. Stylus

We used an MR-safe wooden-tipped stylus, although a number of other MR-safe writing implements could have been used. Participants could easily have used their fingers to interact with the MRItab, for instance.

### 2.1.7. Additional requirements

The use of the MRItab during functional neuroimaging had two additional requirements: an external computer and an open-faced head coil capable of being angled slightly.

*2.1.7.1. External computer.* An external computer was required to interface with the MRItab for the recording and presentation of all experimental stimuli. The external computer connected directly to the Control Box to control the touchscreen and video-display functions of the screen in the Monitor Box. The use of an external computer allowed us to run experiments from a computer that contained all necessary software. The external computer and Control Box necessarily remained in the control room, away from the strong electromagnetic fields in the MRI room.

*2.1.7.2. Angled open-faced head coil.* In order for participants to see the tablet, an open-faced head coil angled upward by about 30 deg was used (Fig. 3). Angling the head coil was only possible with certain head coil designs.[3]

### 2.2. Device testing and validation

### 2.2.1. Safety and device functioning
*2.2.1.1. Design.* To determine whether or not the operation of the MRI affected the operation of the MRItab, we observed the display screen of the MRItab and measured changes in temperature over a certain time window. We compared the temperature of the MRItab before and after scanning and compared the change in temperature to the change in temperature that the MRItab displays if left on over the same period of time when not in the scanner. We, therefore, compared the temperature difference in an MRI condition and in a no-MRI condition. If the operation of the MRI affected the operation of the MRItab, then we should observe interference in the display screen and/or temperature changes in the MRI condition but not in the no-MRI condition. Any temperature changes in the MRI condition would indicate interference and if the temperature changes were high enough, we would be concerned about the safety of the MRI device.

We used copper to shield the electronic components of the MRItab inside the Monitor Box from the radio frequencies emitted during MR imaging. Copper is a weakly diamagnetic material and, consequently, displays some torque when moved through a magnetic field. Importantly, it does not display torque when held in a stationary position. We were concerned, however, that the copper might undergo some heating.

---

[1] In theory, LVDS signals should be tolerant to interference over long cable runs; however, we found that the signals generated by the monitor's original LVDS chip produced major video artifacts, attributable to unacceptably large phase and amplitude distortions over the 9.75 m cable run. This distortion was even evident outside of the MRI-environment. We, therefore, placed cable driver chips at both ends of the cable to alleviate these distortions.

[2] We experimented with positioning the Monitor Box at different angles, but found that angling the MRItab greatly reduced visibility and the amount of room left for a participant's hand and pen. We, instead, decided that the positioning of the MRItab should be perpendicular to the scanner bed.

[3] We used a standard Siemens 32-channel phased array head coil (part number 14436651), although there were other head coil designs that would have also worked.

*2.2.1.2. Procedure.* The temperature was measured at seven surface locations using an infrared thermometer (Manufacturer: Shenzhen Calibeur Industries, Inc, Model: Infrared Thermometer with Laser Targeting, Accession Number: 1520373-000). We selected these locations because they are the only surface locations that were not made of plastic. Six locations were made of copper and the seventh location was the center of the display screen. We measured the temperature at these locations before and after 10 min of functional MRI scanning (see Section 2.3 for scanning parameters) with the device on and powered (i.e., the MRI condition) and before and after 10 min of the device being on and powered but not during MRI scanning (i.e., the no-MRI condition). This was done to ensure that any changes we saw during the MRI condition were not simply due to the general operation of the device, such as the screen heating that typically happens with display devices. The device was removed from the MRI environment before the temperatures were measured. Removal from the MRI environment took approximately 15 s. The temperature of each location was measured twice and then averaged so that we had one temperature for each location in each condition.

Device functioning was assessed by watching the display screen of the MRItab with a camera positioned outside of the bore of the scanner.

*2.2.2. MRI image quality*
*2.2.2.1. Design.* To determine whether or not the operation of the MRItab affected MRI image quality, we tested for differences in image quality under several conditions that varied from the MRItab being absent during image acquisition to the MRItab being present, powered on, and fully functional. Our test conditions were modeled after those recommended by Yu et al. (2011). Yu et al. (2011) recommends that images be collected using a phantom in each of these six conditions: phantom only (pre), device disconnected, device connected, device powered, device functioning, phantom only (post). For our particular device, there was no difference between 'device powered' and 'device functioning' when scanning with a phantom for two reasons: (1) For proper functioning, the MRItab must change its display every few seconds. If a static image is displayed for an extended period of time, the functioning of the MRI may begin to interfere with the display screen. (2) There is no way to collect images during interaction with the touchscreen without a human subject. We also wanted to test the cage and added a step that included only the phantom and the cage. Our six conditions were, therefore: the phantom only (pre), the cage, the cage with the tablet not connected to the Control Box (i.e., the tablet condition), the cage with the tablet connected to the Control Box with no power supplied (i.e., the tabletConnected condition), the cage with the tablet connected to the Control Box with power supplied (i.e., the tabletConnectedOn condition), and the phantom only again with the device removed (post).

*2.2.2.2. Procedure.* We acquired an anatomical image followed by a functional image for each test condition. For each condition, we acquired a functional image to assess the presence of artifacts in the imaging data. Functional data were collected in a series of six steps, similar to the test condition steps described in Yu et al. (2011) for testing image quality. We collected images for these six steps, referred to as Tests, three separate times, referred to as Trials. All images were taken within the same imaging session. For all tests, we used a standard gel phantom made in-house as described in Cheng et al. (2006). The MRItab was affixed to the cage, perpendicular to the static magnetic field, and approximately 35 cm from the phantom.

*2.2.3. Ease of use*
Our aim in developing the MRItab was to construct a digital writing tablet with both touchscreen and video-display capabilities to enable a more ecologically valid study of the neural systems supporting user-tablet interaction. We, therefore, wanted to ensure that the interaction with the MRItab in the supine position that was required with the MRItab apparatus and set-up was not more difficult than interacting with it in the more typical seated position.

*2.2.3.1. Participants.* Three right-handed college-aged adults, 2 male and 2 female of average height and build, were recruited through word of mouth. All participants gave informed consent in accordance with the Indiana University Institutional Review Board.

*2.2.3.2. Design and procedure.* All participants were asked to write all 26 letters of the Roman alphabet, one at a time, on the MRItab outside the MRI in a typical seated position (i.e., the outside-MRI condition) and inside the MRI in the typical supine position (i.e., the inside-MRI condition). As a simple measurement of handwriting ease, we calculated writing duration for each letter. Duration was measured as the time lapse between the first time that the stylus was in contact the tablet to the last time that the stylus was in contact with the tablet, or 'pen down' to 'pen up'.

*2.3. Scanning parameters*

All testing was done in a 3-Tesla Siemens Prisma MRI in the Imaging Research Facility housed in the Department of Psychological and Brain Sciences at Indiana University. High-resolution T1-weighted anatomical volumes were acquired using a Turbo-flash 3-D sequence: TI = 900 ms, TE = 2.7 ms, TR = 1800 ms, flip angle = 9°, with 160 sagittal slices of 1.0 mm thickness, a field of view of 256 × 256 mm, and an isometric voxel size of 1.0 $mm^3$.

For the functional images, the field of view was 220 × 220 mm, with an in-plane resolution of 110 × 110 pixels for a single image and 72 sagittal slices of 2.0 mm thickness per volume with 0% slice gap, producing an isometric voxel size of 2.0 $mm^3$. Multi-band functional images were acquired using a gradient echo EPI sequence with interleaved slice order: TE = 30.40 ms, TR = 1000 ms, flip angle = 52°, multi-band acceleration factor of 6. We collected 40 TRs of functional data from the phantom in order to calculate temporal SNR, as in Carr et al. (2013).

## 3. Results

*3.1. Safety and device functioning*

Temperatures were taken twice at seven different locations and the average temperatures for each location at each test time point are reported in degrees Celsius. One-tailed paired *t*-tests indicated that there was a significant difference in the temperature before and after the 10-minute period in both the MRI condition, $t(6) = 8.50$, $p < 0.001$, and in the no-MRI condition, $t(6) = 4.42$, $p < 0.01$. For the MRI condition, the temperature was greater after the 10-minute period ($M = 23.54$, $SD = 1.43$) than before ($M = 21.19$, $SD = 0.69$). For the no-MRI condition, the temperature was also greater after the 10-minute period ($M = 23.06$, $SD = 1.18$) than before ($M = 20.81$, $SD = 0.48$).

To ensure that the temperature increase in the MRI condition was no greater than the temperature increase in the no-MRI condition, we subtracted the after temperatures from the before temperatures to quantify the temperature change in each condition. We found no significant difference between the temperature change in the MRI condition ($M = 2.35$, $SD = 0.83$) and the temperature change in the no-MRI condition ($M = 2.26$, $SD = 1.57$), $t(6) = 0.26$, $p = 0.80$, indicating that the functioning of the scanner did not induce additional heating in the MRItab.

We did not visually observe any interference in the functioning of the MRItab during any of the functional imaging sessions. All images displayed with full color and resolution without distortion during all tests and trials.

## 3.2. MRI image quality

To determine whether or not the operation of the MRItab had any effects on functional image quality, we first determined whether any spatial distortions existed. We followed this initial procedure by (1) performing a voxel-wise comparison of the signal values of the functional images collected in each condition, (2) comparing the spatial signal-to-noise ratio (sSNR) for the functional images collected in each condition, (3) comparing the temporal signal-to-noise ratio (tSNR) for the functional images collected in each condition, and (4) ensuring that the tSNR values during the use of the tablet were sufficient to detect effects in a typical psychological study.

By visually inspecting the functional data, we observed that no obvious spatial distortions existed. Due to the absence of obvious spatial distortion, the following analyses were performed on a region of interest (ROI), as in other studies (e.g., Carr et al., 2013; Diciotti et al., 2010; Tam et al., 2011; Suminski and Scheidt, 2014). For our ROI, we selected a large 40 × 40 × 40 voxel cube centered at (x, y, z) = (55, 55, 36) in LPS image space.

### 3.2.1. Magnitude time course

A voxel-wise general linear model (GLM) with one predictor of interest for each condition was constructed and a Random-effects GLM analysis was performed on the functional data. We collapsed across Trial, repeats of each Test condition, because we were interested in differences between Test conditions and not an interaction. We performed direct comparisons between the resulting statistical maps for each test condition.

We first compared phantom (pre) to phantom (post) to ensure that there were no differences attributable to scanner instabilities. We then compared (1) the tabletConnectedOn test condition to the tabletConnected test condition to determine if differences in the signal arose from power being supplied to the MRItab, (2) the tabletConnected test condition to the tablet test condition to determine if differences in the signal arose from the tablet being connected to other electronic devices, (3) the tablet test condition to the cage test condition to determine if differences in the signal arose from the presence of the tablet, (4) the cage test condition to the phantom (pre) test condition to determine if differences in the signal arose from the presence of the cage, and (5) the tabletConnectedOn test condition to the phantom (pre) test condition to determine if differences in the signal existed between the full functioning of the MRItab and a completely baseline state. Resulting t-maps were subjected to a liberal voxel-wise threshold of $p_{voxel} < .25$. We found no difference in signal magnitude for any comparison.

### 3.2.2. Spatial SNR

With no interference from the MRItab, we would expect the signals recorded from the phantom to remain consistent across voxels. We used the following equation to calculate sSNR for each time point (i.e., TR):

$$sSNR = \frac{mean \ (S_t)}{standard \ deviation (S_t)}$$

where $S_t$ is the signal magnitude of all voxels within the ROI at a particular time point (i.e., TR). We calculated the sSNR for each of the 40 functional TRs acquired for each condition. A mixed general linear model was constructed with one predictor for each of the six Test levels (i.e., phantom (pre), cage, tablet, tabletConnected, tabletConnectedOn, phantom (post)). Test was treated as a fixed-effect and TR was treated as a random-effect. sSNR was the dependent measure. sSNR values for all conditions are reported in Table 1.

The linear mixed model revealed a main effect of Test, $F$(5, 718) = 994009, $p < .001$ (Fig. 4). Bonferroni-corrected post hoc paired t-tests revealed that sSNR was *greater* in the tablet condition ($M = 363$, $SD = 2.51$) than during the cage condition ($M = 355$, $SD = 1.75$), $p < .001$, the phantom (pre) condition ($M = 356$, $SD = 1.99$), $p < .01$,

and the phantom (post) condition ($M = 356$, $SD = 2.15$), $p < .001$. The post hoc tests also revealed that sSNR during the tabletConnected condition ($M = 363$, $SD = 2.45$) was greater than sSNR during the phantom (post) condition ($M = 356$, $SD = 2.15$), $p < .05$. There were no differences between tablet, tabletConnected, and tabletConnectedOn conditions. There was no difference between phantom (pre) and phantom (post).

### 3.2.3. Temporal SNR

Temporal SNR is the primary SNR value of interest in most fMRI studies because fMRI analyses rely upon the ability to detect a difference in the signal from one time point to another. Differences in SNR across time are the most likely to cause false positives in fMRI experiments. With no interference from the MRItab, we would expect the signal to remain relatively consistent across the 40 time points. We used the following equation to calculate tSNR for each voxel:

$$tSNR = \frac{mean \ (S_v)}{standard \ deviation \ (S_v)}$$

where $S_v$ is the signal magnitude across time of a particular voxel. We calculated tSNR for each voxel in the ROI for each condition. A mixed general linear model was constructed with one predictor for each of the six test conditions (i.e., phantom (pre), cage, tablet, tabletConnected, tabletConnectedOn, phantom (post)). Test was treated as fixed-effects and voxel was treated as a random-effect. tSNR was the dependent measure. tSNR values for all conditions are reported in Table 2.

The linear mixed model revealed a main effect of Test, $F$(5, 1068000) = 1223236, $p < .0001$ (Fig. 5). Bonferroni-corrected post hoc paired t-tests revealed that tSNR was *lower* in the tabletConnectedOn ($M = 2462$, $SD = 648$) condition than in the phantom (pre) ($M = 2621$, $SD = 667$), $p < .001$, cage ($M = 2622$, $SD = 667$), $p < .001$, and phantom (post) ($M = 2617$, $SD = 665$), $p < .001$, conditions. The tSNR was also greater in the tabletConnected condition ($M = 2511$, $SD = 632$) than in the tablet condition ($M = 2504$, $SD = 630$), $p < .05$, and than in the tabletConnectedOn condition, $p < .001$.

### 3.2.4. SNR analysis

The statistical differences in tSNR and sSNR demonstrate that the MRItab caused a measureable decrease in SNR. Even though the decrease was statistically significant, both SNR measures remained relatively high for all conditions. Another important step was, therefore, to determine if the SNR values with the MRItab were high enough to effectively detect differences between typical experimental conditions in a human fMRI study. We focused on tSNR because most fMRI studies are interested in condition differences across time. We did not perform the analysis on sSNR because the variance across voxels was approximately zero, indicating that task-evoked activation at each voxel location had a similar chance of being detected at any particular time point. tSNR, furthermore, was the only one of the two SNR values that *decreased* during the tablet conditions.

We, therefore, calculated the minimum tSNR needed to detect a difference between hypothetical experimental conditions for a range of sample sizes and effect sizes at 80% power, using a similar simulation as Wakefield et al. (2013). The protocol for the simulation was based on a typical blocked design with 7 conditions in which each condition was repeated twice within one functional run. Blocks were 30 s with 10-second inter-block intervals. Simulated time courses were sampled every 2 s to imitate a 2-second TR.

We found that tSNR values of 163 or greater were sufficient to detect a small effect in a single participant (Table 3). This value is similar to the values reported in Wakefield et al. (2013) and to the values reported for a similar study design in Parrish et al. (2000) for a 1.5 T MRI. The mean tSNR value measured with the phantom was 2462 during the tabletConnectedOn condition. In sum, although tSNR was statistically lower during the tabletConnectedOn condition than during the

**Table 1**

Spatial Signal-to-noise Ratio (sSNR). Calculated sSNR values and standard deviation for a 40 × 40 × 40 voxel cube centered at (x, y, z) = (55, 55, 36). Bolded values are the means (M) and standard deviations (SD) for each Trial (row) and Test (column).

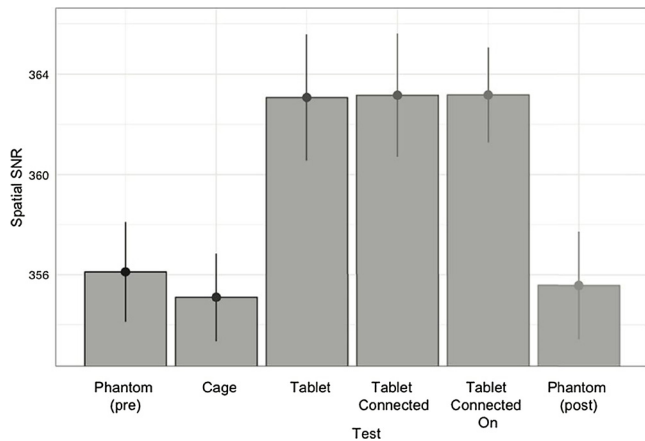| | Phantom (pre) M (SD) | Cage M (SD) | Tablet M (SD) | Tablet Connected M (SD) | Tablet Connected On M (SD) | Phantom (post) M (SD) | |
|---|---|---|---|---|---|---|---|
| Trial 1 | 354 (0.23) | 353 (0.25) | 360 (0.30) | 361 (0.32) | 361 (0.65) | 353 (0.29) | **357 (3.73)** |
| Trial 2 | 356 (0.26) | 356 (0.27) | 363 (0.28) | 362 (0.31) | 364 (0.30) | 358 (0.31) | **360 (3.35)** |
| Trial 3 | 359 (0.29) | 357 (0.26) | 366 (0.28) | 366 (0.33) | 365 (0.35) | 356 (0.31) | **361 (4.56)** |
| | **356 (1.99)** | **355 (1.75)** | **363 (2.51)** | **363 (2.45)** | **363 (1.89)** | **356 (2.15)** | |



**Fig. 4.** Spatial SNR by Test.
Mean and standard deviation of the *sSNR* value in a 40 × 40 × 40 voxel cube placed in the center of the phantom for each of the six test conditions. A linear mixed model revealed a main effect of Test, $F(5, 718) = 994009$, $p < .001$. Bonferroni-corrected post hoc paired t-tests revealed that *sSNR* was *greater* in the tablet condition ($M = 363$, $SD = 2.51$) than during the cage condition ($M = 355$, $SD = 1.75$), $p < .001$, the phantom (pre) condition ($M = 356$, $SD = 1.99$), $p < .01$, and the phantom (post) condition ($M = 356$, $SD = 2.15$), $p < .001$. The post hoc tests also revealed that *sSNR* during the tabletConnected condition ($M = 363$, $SD = 2.45$) was greater than *sSNR* during the phantom (post) condition ($M = 356$, $SD = 2.15$), $p < .05$. There were no differences between tablet, tabletConnected, and tabletConnectedOn conditions. There was no difference between phantom (pre) and phantom (post). Note that the *sSNR* values ranged between 356 in the phantom conditions and 363 in the tablet conditions, indicating that the presence of the tablet only increased *sSNR* by a factor of 1.02, or 2%.

phantom conditions (i.e., phantom (pre), phantom (post)), it was still well above the minimum *tSNR* necessary to uncover statistical differences between experimental conditions in a typical psychological fMRI experiment.

### 3.3. Ease of use

The average duration outside the MRI was 1.98 s with a standard deviation of 0.61. The average duration inside the MRI was 2.00 s with a standard deviation of 0.63. A paired *t*-test revealed that there were no significant differences in the amount of time it took participants to write letters outside the MRI in the seated position and the amount of
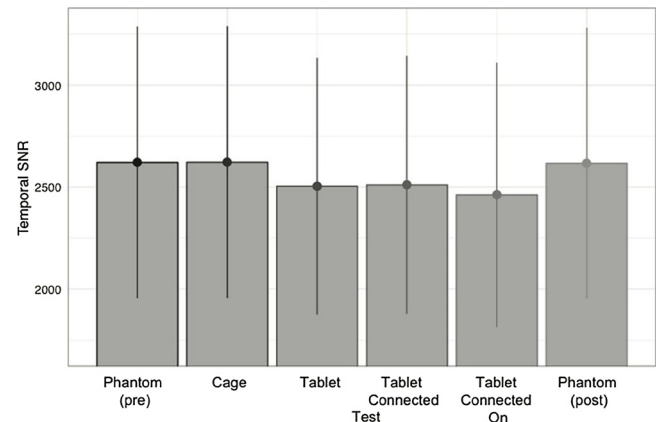


**Fig. 5.** Temporal SNR by Test.
Mean and standard deviation of the *tSNR* value in a 40 × 40 × 40 voxel cube placed in the center of the phantom for each of the six test conditions. A linear mixed model revealed a main effect of Test, $F(5, 1068000) = 1223236$, $p < .0001$. Bonferroni-corrected post hoc paired t-tests revealed that *tSNR* was *lower* in the tabletConnectedOn ($M = 2462$, $SD = 648$) condition than in the phantom (pre) ($M = 2621$, $SD = 667$), $p < .001$, cage ($M = 2622$, $SD = 667$), $p < .001$, and phantom (post) ($M = 2617$, $SD = 665$), $p < .001$, conditions. The *tSNR* was also greater in the tabletConnected condition ($M = 2511$, $SD = 632$) than in the tablet condition ($M = 2504$, $SD = 630$), $p < .05$, and than in the tabletConnectedOn condition, $p < .001$. Note that the *tSNR* values ranged between 2630 in the phantom conditions and 2398 in the tablet conditions, indicating that the presence of the tablet only decreased *tSNR* by a factor of 1.08, or 8%.

**Table 3**

Minimal tSNR for Various n-values and Effect Sizes. The minimal *tSNR* required to detect a change in the MR signal for a range of effect and sample sizes with 80% power at the $p < .01$ significance threshold. The highest *tSNR* necessary was 163 to detect a small effect in only one participant.

Minimal tSNR for Various n-values and Effect Sizes

| | | n-values | | | |
|---|---|---|---|---|---|
| | | 1 | 5 | 10 | 15 |
| *Effect Sizes* | small | 163 | 145 | 145 | 130 |
| | medium | 146 | 104 | 76 | 65 |
| | large | 132 | 76 | 57 | 52 |

**Table 2**

Temporal Signal-to-noise Ratio (tSNR). Calculated tSNR values and standard deviation for a large 40 × 40 × 40 voxel cube centered at (x, y, z) = (55, 55, 36). Bolded values are the mean (M) and standard deviations (SD) for each Trial (row) and Test (column).

| | Phantom (pre) M (SD) | Cage M (SD) | Tablet M (SD) | Tablet Connected M (SD) | Tablet Connected On M (SD) | Phantom (post) M (SD) | |
|---|---|---|---|---|---|---|---|
| Trial 1 | 2623 (660) | 2621 (657) | 2473 (615) | 2489 (619) | 2398 (650) | 2630 (650) | **2539 (649)** |
| Trial 2 | 2619 (670) | 2625 (670) | 2505 (635) | 2514 (638) | 2489 (645) | 2612 (670) | **2561 (656)** |
| Trial 3 | 2621 (670) | 2621 (673) | 2535 (637) | 2529 (639) | 2501 (645) | 2609 (674) | **2569 (658)** |
| | **2621 (667)** | **2622 (667)** | **2504 (630)** | **2511 (632)** | **2462 (648)** | **2617 (665)** | |

time it took them inside the MRI in the supine position, $t(2) = 0.52$, $p = 0.83$.

## 4. Discussion

Combining video-display and touchscreen technologies for use in an MRI environment requires the development of new technologies that are capable of functioning in a strong electromagnetic environment. Several video-display devices have been developed for use outside of the bore of the MRI and touchscreen devices have been developed for use inside the bore of the magnet but, until now, no device has been able to combine video-display and touchscreen technologies into an MRI-compatible device. We have described the development and validation of the MRItab, the first such device. The MRItab makes use of special signal-driver circuitry and shielding to combine these two technologies into an MR-compatible device. We have demonstrated that the functioning of the MRItab is not affected by the operation of the MRI, that the operation of the MRI is not affected by the functioning of the MRItab to a point that jeopardizes the ability of experimenters to detect effects in typical fMRI experiments, and that participants can use the MRItab with ease in an MRI environment.

### 4.1. Safety and device functioning

All electronic devices undergo some level of heating during operation. We wanted to ensure that the heating of the MRItab during operation, during scanning and outside of scanning, would not cause burns. Burns may be caused by prolonged exposure to materials at or greater than 43 deg Celsius or very brief exposures to materials at or greater than 80 deg Celsius. We found that all temperatures recorded after device functioning were well below this temperature (e.g., 23.54 deg Celsius) and, further, that there was no difference in the heating that occurred due to device functioning outside of the MRI and the heating that occurred inside the MRI. This indicates that the MRItab does not undergo heating when used during MRI scanning beyond what would normally be expected from an electronic device and, further, that any heating that does occur is not so great that it causes any safety concerns.

Finding no substantial increase in temperature also indicates that the functioning of the scanner was not interfering with the functioning of the device. We also never observed any image display problems during functional imaging. These results, together, indicate that the functioning of the MRI does not interfere with the functioning of the MRItab.

### 4.2. MRI image quality

#### 4.2.1. Magnitude images
Functional neuroimaging uses the magnitude of the MR signal to infer task-based differences in brain function. It was, therefore, extremely important to demonstrate that the MRItab does not affect this component of the signal. We found no differences between any conditions in the magnitude of the MRI signal at any voxel location, indicating that the measurement of the MR signal is not affected by the functioning of the MRItab during scanning.

#### 4.2.2. Spatial SNR
While having the device present did seem to affect *sSNR*, the differences were very small. The *sSNR* in each of the tablet conditions (i.e., tablet, tabletConnected, tabletConnectedOn) was 363. The *sSNR* in each of the phantom conditions (i.e., phantom (pre), phantom (post)) was 356 and the *sSNR* in the cage condition was not significantly different. The presence of the MRItab, therefore, only increased the *sSNR* by a factor of 1.02, or 2%.

The presence of the device, not connected, connected, and/or powered on, actually *increased sSNR*. This was an unexpected result. We

expected that if any effect occurred due to the presence of the MRItab, that the effect would be a reduction in *sSNR* due to an increase in the noise of the measurement. The increase in *sSNR* was due to a decrease in the standard deviation of the signal, as there were no differences in the mean signal value between conditions. We are unsure why the presence of the MRItab had such an effect. A similar increase in *SNR* is reported in Suminski and Scheidt (2014) for two out of seven regions of interest placed at various distances from their device. The fact that the difference only occurred at some locations indicated that small variations in the noise of the signal across space occur naturally, because they were not systematically related to the distance of the ROI from their electronic device. Further work is necessary to understand this result, but it is clear that the presence of the cage and the MRItab does not reduce *sSNR*.

#### 4.2.3. Temporal SNR
We found that the presence of the tablet in the bore of the scanner, whether connected and/or powered on, significantly decreased the *tSNR* of the image according to statistical criteria. The *tSNR* change, however, was very small in practical terms. *tSNR* ranged from 2398 to 2630. The 2398 *tSNR* value occurred with the entire apparatus and MRItab connected and fully functioning and the 2630 *tSNR* value occurred with only the phantom present. The presence of the cage and a fully functioning tablet, therefore, resulted in a decrease in *tSNR* by only a factor of 1.08, or 8%. In general, an 8% decrease in *tSNR* is very low and, paired with the exceptionally high *tSNR* values, should have no meaningful effect on the ability to detect effects in a typical psychological fMRI study.

#### 4.2.4. SNR analysis
All *tSNR* values were magnitudes above the *tSNR* required to detect an effect in a typical fMRI study, even for a sample size of one. Our SNR analysis, therefore, confirmed that the small changes observed in *tSNR* would have no meaningful effect on the ability to detect effects in a typical fMRI studies.

### 4.3. Ease of use

Writing duration is a simple measurement of writing ease. We found no difference in writing duration between letters written on the MRItab in the supine and head-angled position and the typical seated posture, indicating that the writing posture required with the MRItab apparatus and set-up has ecological validity.

### 4.4. Limitations

Our safety and device functioning assessments indicate that the MRItab is safe for use in the MRI environment. More extensive testing exists, however. This additional testing is commercially available and includes formal torque measurements, for instance.

We have performed our analyses using a Siemens 3 T Prisma scanner with a standard pulse sequence for functional imaging. The compatibility of the MRItab with this scanner and sequence does not guarantee compatibility with other scanners, field strengths, and pulse sequences. Our results should hold in other Siemens 3 T Prisma scanners with similar functional sequences, but future work will need to be done to determine compatibility of the MRItab with other field strengths, such as 1.5 T and 7.0 T, and with other pulse sequences, such as diffusion imaging and spectroscopy.

## 5. Conclusions

Here, we present the first MR-compatible computer tablet with video-display and touchscreen capabilities designed for use in the MRI environment. The MRItab and holding apparatus can be made from easy-to-attain, off-the-shelf materials that are inexpensive relative to

other MR-compatible devices. Our testing demonstrated that the functioning of the MRItab was not affected by the functioning of the MRI scanner. The MRItab did not undergo heating and no interference in the visual display was observed during MRI scanning. Our testing also demonstrated that the MRItab did not adversely affect the image data acquired. The signal magnitude was not affected and SNR was not affected in any practical manner. The MRItab is, furthermore, an interactive digital device that allows participants to see their hands directly (instead of through a system of mirrors) as they interact with the tablet resulting in high ecological validity. The MRItab is, therefore, the first truly interactive tablet that can be implemented in MRI experiments.

## Conflict of interest statements

This report describes development and validation of an MRI-compatible device that received a provisional patent from the United States in 2016: Sturgeon, J., Shroyer, A., Vinci-Booher, S., & James, K.H., applicants (filed August 3rd, 2016). Electronic tablet for use in functional MRI. *US Patent Application No. 62/370, 372*. As the patent was provisional, there were no commercial or financial conflicts of interest during the procedures described in this report or during the writing of this report.

## Acknowledgements

## References

Carr, S.J., Borreggine, K., Heilman, J., Griswold, M., Walter, B.L., 2013. Novel magnetomechanical MR compatible vibrational device for producing kinesthetic illusion during fMRI. Med. Phys. 40 (11), 112303. http://dx.doi.org/10.1118/1.4824695.

Cheng, H., Zhao, Q., Duensing, G.R., Edelstein, W.A., Spencer, D., Browne, N., et al., 2006. SmartPhantom—an fMRI simulator. Magn. Reson. Imaging 24 (3), 301–313. Retrieved from. http://www.sciencedirect.com/science/article/pii/S0730725X05003772.

Diciotti, S., Cecchi, P., Ginestroni, A., Mazzoni, L.N., Pesaresi, I., Lombardo, S., et al., 2010. MR-compatible device for monitoring hand tracing and writing tasks in fMRI with an application to healthy subjects. Concepts Magn. Reson. Part A Bridging Educ. Res. 36 (3), 139–152. Retrieved from. http://onlinelibrary.wiley.com/doi/10.1002/cmr.a.20158/full.

James, K.H., Gauthier, I., 2006. Letter processing automatically recruits a sensory–motor brain network. Neuropsychologia 44 (14), 2937–2949. http://dx.doi.org/10.1016/j.neuropsychologia.2006.06.026.

Karimpoor, M., Tam, F., Strother, S.C., Fischer, C.E., Schweizer, T.A., Graham, S.J., 2015. A computerized tablet with visual feedback of hand position for functional magnetic resonance imaging. Front. Hum. Neurosci. 9, 150. http://dx.doi.org/10.3389/fnhum.2015.00150.

Katanoda, K., Yoshikawa, K., Sugishita, M., 2001. A functional MRI study on the neural substrates for writing. Hum. Brain. Mapp. 13 (1), 34–42. Retrieved from. https://www.ncbi.nlm.nih.gov/pubmed/11284045.

Mraz, R., Ferber, S., Baker, S.N., Graham, S.J., 2004. An fMRI-compatible writing device for investigating the neural substrates of drawing, copying and tracing. Proc. Int. Soc. Magn. Reson. Med. 12, 1042.

Parrish, T.B., Gitelman, D.R., LaBar, K.S., Mesulam, M., 2000. Impact of signal-to-noise on functional MRI. Magn. Reson. Med. 44 (6), 925–932.

Reitz, F., Richards, T., Wu, K., Boord, P., Askren, M., Lewis, T., Berninger, V., 2013. A low-cost, computer-interfaced drawing pad for FMRI studies of dysgraphia and dyslexia. Sensors 13 (4), 5099–5108.

Suminski, A., Scheidt, R., 2014. Feedback regulation of limb position characterized using FMRI. Advanced Brain Neuroimaging Topics in Health and Disease-Methods and Applications. InTech Retrieved from. https://www.intechopen.com/books/advanced-brain-neuroimaging-topics-in-health-and-disease-methods-and-applications/feedback-regulation-of-limb-position-characterized-using-fmri.

Tam, F., Churchill, N.W., Strother, S.C., Graham, S.J., 2011. A new tablet for writing and drawing during functional MRI. Hum. Brain. Mapp. 32 (2), 240–248. Retrieved from. http://onlinelibrary.wiley.com/doi/10.1002/hbm.21013/full.

Wakefield, E.M., James, T.W., James, K.H., 2013. Neural correlates of gesture processing across human development. Cognit. Neuropsychol. 30 (2), 58–76. http://dx.doi.org/10.1080/02643294.2013.794777.

Yu, N., Gassert, R., Riener, R., 2011. Mutual interferences and design principles for mechatronic devices in magnetic resonance imaging. Int. J. Comput. Assisted Radiol. Surg. 6 (4), 473–488. http://dx.doi.org/10.1007/s11548-010-0528-2.